Hyperspectral spatially offset Raman spectroscopy in a microfluidic channel

Matthiae, Moritz; Kristensen, Anders

Published in:
Optics Express

Link to article, DOI:
10.1364/OE.27.003782

Publication date:
2019

Document Version
Publisher's PDF, also known as Version of record

Research Article | Vol. 27, No. 3 | 4 Feb 2019 | OPTICS EXPRESS 3782
Optics EXPRESS

Hyperspectral spatially offset Raman spectroscopy in a microfluidic channel

MORITZ MATTHIAE[1] AND ANDERS KRISTENSEN[1,2,*]

[1]*Department of Micro- and Nanotechnology, Technical University of Denmark, 2800 Kongens Lyngby, Denmark*
[2]*Department of Health Technology, Technical University of Denmark, 2800 Kongens Lyngby, Denmark*
[*]*akri@dtu.dk*

Abstract: Spatially offset Raman spectroscopy (SORS) enables one to distinguish chemical fingerprints of top and subsurface layers. In this paper, we apply SORS to a microfluidic two-layer system consisting of transparent liquid in a microchannel as the surface layer and microfluidic PDMS chip material as the sublayer. By using an imaging spectrograph connected to a microscope, we perform hyperspectral SORS acquisitions. Furthermore, the focus position z is translated. Thus, we combine the two methods of hyperspectral SORS and defocusing micro-SORS, which leads to an integral characterization of the layered system. The collected top and subsurface layers of Raman scattering at the optical axis (zero spatial offset) largely depends on the focus position z. However, the spatially offset Raman scattered intensity from the subsurface layer is constant for a large range of focus positions z. We claim that there is potential for internal referencing and alignment reproducibility. We demonstrate these findings experimentally in a microfluidic scenario where a 16 μm deep channel is filled with an aqueous hemoglobin solution. Our observation enables consistent concentration measurements in small-volume liquid samples.

1. Introduction

Spatially offset Raman spectroscopy (SORS) enables the chemical distinction of top and subsurface layers in stacked systems. Raman scattered photons are collected at a spatially offset position relative to the position of laser excitation. Raman scattered photons from deeper layers appear as an extended pattern at the surface whereas Raman scattered photons from the top layer are more localized [1–3]. This allows the exclusive detection of Raman scattered photons from deeper layers at large spatial offsets. The top layer Raman signature can be reobtained by a weighted subtraction of the deeper layer signature [3]. The conventional, fiber-based SORS technique is capable of depth analysis in turbid media at depth of 1-10 mm [4] and micro-SORS enables analysis down to below 100 μm [5] depending on the investigated materials.

SORS has attracted major interest in recent years. Applications include studies on drug detection inside Raman active containers [4], multi paint layers in art restaurations [6], wheat seeds [7], bones [8], tissue [9] and toxic chemicals inside building materials [10], for examples. In fiber offset Raman spectroscopy - the most widely applied SORS technique - the Raman excitation fiber and the collection fiber are separated by an adjustable distance on the order of some millimeters. In micro-SORS, the offset Raman signal at the sample surface is collected only some micrometres from the pump beam. The imaging system of the Raman microscope maps this signal onto the imaging CCD camera. Conti et al. [11] and Matousek et al. [5] investigated the effect when defocusing the Raman microscope, thereby enlarging Raman excitation and collection zones on turbid, layered samples. Furthermore, Raman microscopy in combination with an imaging spectrometer and a slit as field aperture enables hyperspectral Raman acquisitions. Such a system can be used for line-scan spatially offset Raman mapping [12].

In the present study, we combine defocusing micro-SORS and hyperspectral Raman imaging to demonstrate quantitative Raman analysis in microfluidic samples. Raman spectroscopy applied

#354882 https://doi.org/10.1364/OE.27.003782
Journal © 2019 Received 7 Dec 2018; revised 14 Jan 2019; accepted 21 Jan 2019; published 1 Feb 2019

Optics EXPRESS

to microfluidics [13] benefits from little sample consumption and convective heat dissipation supporting Raman analysis of liquid biological and biomedical samples as blood and other body fluids. Furthermore, surface-enhanced Raman spectroscopoy (SERS) by means of metallic colloidal solutions finds application in Raman microfluidics as reviewed by Jahn et al [14]. Manipulation schemes of microfluidic flow [15] as well as reduced consumption of both analyte and colloidal nanoparticles are key advantages. On the other hand, linearity and reproducibility are in general limitations in quantitative Raman analysis of liquids. Linearity is undermined by liquid sample absorption [16]. But the problem can be overcome in microfluidics by a short optical interaction length in shallow channels. Reproducibility can be limited by unstable optical alignment or inhomogeneous analyte distribution which occurs in particular in dried samples.

In this manuscript we use a microscope-based hyperspectral spatially offset Raman spectrometer which probes a two-layer microfluidic system. We distinguish the two layers by their Raman signatures: The analyte in the channel is an aqueous hemoglobin solution with clear Resonance Raman scattering in the fingerprint region. The microfluidic chip material is PDMS with another characteristic Raman signature at higher wavenumbers. We perform z-scans of the hyperspectral Raman acquisition and observe the collected Raman scattering both at the position of the laser excitation and at a continuous set of spatially offset positions. We find potential for intensity calibration and alignment correction in microfluidic Raman experiments.

2. Experimental methods

Microfluidics Aqueous hemoglobin solutions are prepared by diluting lyzed whole blood (SSI Diagnostica A/S, Hillerod, Denmark) with water. All animal procedures are performed in accordance with the EU-directive on the protection of animals used for scientific purposes as well as the Danish order regarding animal experimentation, and approved by the Danish Veterinary and Food Administration. In advance, hemoglobin concentrations in undiluted whole blood are determined with a blood-gas analyzer (ABL-90, Radiometer Medical Aps, Copenhagen, Denmark) to be 130 g/l. Final hemoglobin concentrations span the range 0-3.5 g/l.

We fabricate rectangular microfluidic channels of 100 μm in width, 16 μm in height and 9 mm in length in polydimethylsiloxane (PDMS). The silicon master is manufactured by UV-lithography and Deep Reactive Ion Etching. After PDMS casting and 3 hours of curing at 75 degrees, fluidic inlet and outlet are introduced with a biopsy punch into PDMS. Oxygen plasma enables consistent bonding to a glass slide. The liquid sample is placed in the inlet reservoir. An underpressure of 1-10 mbar applied to the outlet achieves constant flow for up to several hours.

Raman equipment The microfluidic PDMS chip is mounted on the translation stage of an inverted microscope (Nikon-Ti, Shinagawa, Japan) with a 60x air objective (NA 0.85, WD 300 μm). The optical setup is shown in Fig. 1(a). All axes of the motorized stage can be adjusted with 0.1 μm accuracy. For Raman excitation, a collimated beam from a diode laser at 406 nm (Toptica, Munich, Germany) is coupled into the microscope and focused by the objective to a small spot in the field of view. The laser power at the sample is 1.6 mW. The sidebands of the diode laser are filtered by an appropriate insertable laser line filter.

The field of view is imaged by a Shamrock 303i imaging spectrometer, equipped with a Newton 920 deep-cooled back-illuminated CCD camera (Andor Technology, Belfast, Northern Ireland). The position of the focused laser spot in the field of view is adjusted such that it enters the spectrometer through the insertable 100 μm entrance slit.

A Notch filter (NF405-13, Thorlabs) allows only inelastically scattered intensity to enter the spectrometer. The spectrometer grating (1200 lines/mm) achieves a horizontal spectral distribution of focused Raman intensity onto the CCD camera. However, different vertical positions on the CCD camera report Raman scattering at different spatial positions y along the spectrometer slit in the field of view. These positions y are spatially offset from the laser

Optics EXPRESS

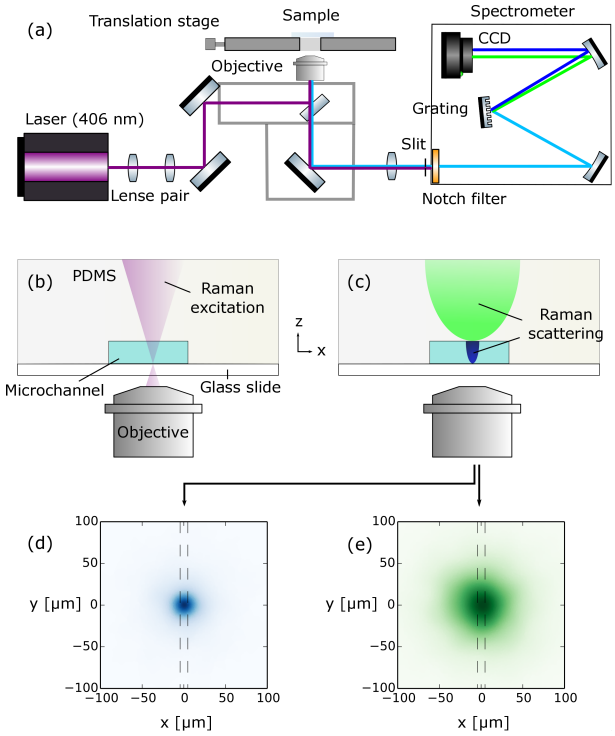

Fig. 1. (a) Raman spectroscopy microfluidic setup. (b) Focused laser beam entering the two-layer system: liquid sample in microchannel and PDMS chip material. (c) The resulting scattered light response. (d-e) Microscope images of scattered light, in focus with the bottom of the microfluidic channel. The optical axis of the excitation laser beam is at Origo. The vertical dashed lines represent the entrance aperture of the imaging spectrometer.

excitation which is at $y = 0\,\mu$m. Spatially offset Raman intensity reports scattering from sample volume that is not in focus with the image plane of the microscope.

In our study, we evaluate the spectrometer CCD images with spectral dispersion in one dimension and the spatial coordinate in the other dimension. The spatial selection in the image plane is made by the spectrometer entrance slit. Our optical detection setup is identical to a line-scan Raman spectrometer [17].

3. Results and discussion

The microfluidic system is illustrated in Figs. 1(b-c). Raman interaction volumes are differently sized: While Raman scattering from hemoglobin is localized (blue), Raman scattering from the PDMS chip (green) extents far more. In particular, the lateral extent of Raman scattering is different, as shown in microscope images with the focus onto the bottom of the microfluidic channel in Figs. 1(d-e).

The overall Raman response is characterized by two distinct signatures as presented in Fig. 2(a). The Resonant Raman spectrum of hemoglobin [18] has a very dominant peak at about 1375 cm^{-1}. In contrast, the PDMS Raman spectrum [19] has a strong peak at about 2920 cm^{-1}. We find both signatures in horizontal orientation in the hyperspectral Raman acquisition of Fig. 2(b).

Raman intensity at small spatial offsets incorporates the hemoglobin signature from the channel. At larger offsets Raman scattering from the channel is suppressed and only the PDMS signature

Optics EXPRESS

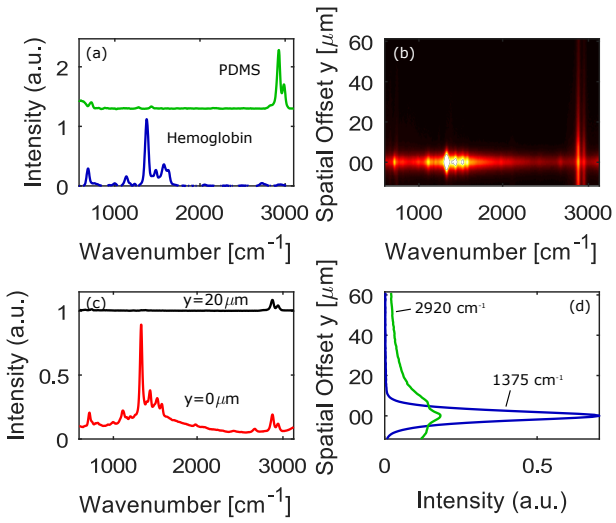

Fig. 2. (a) Raman spectra of PDMS (green) and hemoglobin (blue), for reference. (b) Hyperspectral Raman CCD image recorded with the imaging spectrometer. Each row represents a Raman spectrum at a different postion (spatial offset y) along the length of the spectrometer entrance slit. The vertical spatial coordinate has origo at the optical axis of the laser beam. (c) Derived crosssection spectra at y=0 μm (red) and y=20 μm (black) spatial offset. (d) Intensity profiles at wavenumbers 1375 cm^{-1} (blue) and 2920 cm^{-1} (green).

from larger depth is present. Figure 2(c) shows horizontal cross-sectional Raman spectra derived from Fig. 2(b) at the offsets $y = 0$ μm and $y = 20$ μm.

We also derive Raman intensity profiles at fixed wavenumbers, as function of the spatial offset coordinate. Here, the hemoglobin signal (1375 cm^{-1} in blue) decays strongly towards larger spatial offset with respect to the excitation at $y = 0$ μm. The PDMS signal (2920 cm^{-1} in green) appears defocused and its intensity decreases only weakly towards larger spatial offset. Thus, PDMS Raman intensity is also present at large spatial offsets. We would like to emphasize that these findings are consistent with the illustration in Figs. 1(d-e): The collected scattered intensity in the vertical y coordinate is very localized regarding scattering from the channel, whereas the collected out-of-focus scattering from the PDMS material is laterally extended in the image plane.

Figure 3 shows spatially offset hyperspectral CCD acquisitions for three different focus positions z as depicted in the diagrams on the left, respectively. At each focus position z the collection optics are in focus with a specific plane of the layered stack. When the focus z is adjusted to be inside the channel, we detect in-focus Raman scattering from the channel and out-of-focus Raman scattering from the PDMS material. As soon as the focus z moves from the channel into the PDMS material, the Raman scattering from the channel is out of focus and Raman scattering from PDMS is in focus. In practice, these transitions are not sharp due to a non-zero depth of field of the microscope objective.

When the focus z is at the bottom of the channel in Fig. 3(a), we see a moderate hemoglobin Raman intensity and a weak in-focus PDMS Raman intensity. As z is moved upwards, the hemoglobin intensity has a maximum for z being at the channel center. At the same time, the in-focus PDMS intensity increases monotonically as z is moved towards the channel-PDMS interface.

However, the spatially offset PDMS Raman intensity is constant at all three positions z that

Optics EXPRESS

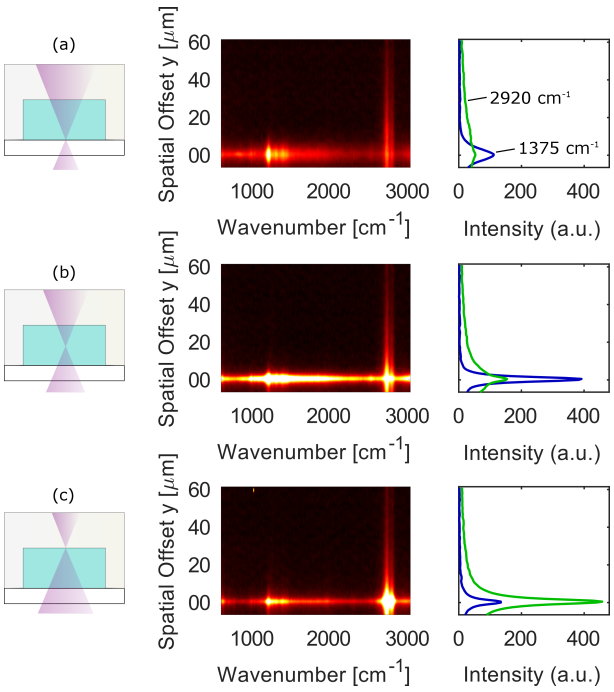

Fig. 3. Hyperspectral spatially offset Raman acquisitions at three different focus positions z and respective spatial profiling at wavenumbers 1375 cm^{-1} of hemoglobin (blue) and 2920 cm^{-1} of PDMS (green). (a-b) Focused to $z = -8\,\mu$m at the bottom of the channel. (c-d) Focused to $z = 0\,\mu$m at the middle of the channel. (e-f) Focused to $z = 8\,\mu$m at the top of the channel.

are shown in Fig. 3. This intensity reports Raman scattering in PDMS of larger depth. The mean-free path length of photons in transparent PDMS is long so that a loss of memory happens regarding the location where the initial laser photon entered. Thus, the spatially offset PMDS Raman intensity appears as a constant background which does not change due to a few micrometer variation of the focus position z. Figure 4(a) underlines this finding by comparing PDMS Raman intensity profiles at various focus positions z. There are large deviations in PDMS Raman intensity at zero spatial offset $y = 0\,\mu$m . Nevertheless, PDMS Raman intensity is constant at large spatial offsets for all measured focus positions z. Figure 4(b) shows the PDMS Raman intensity at $y = 40\,\mu$m (light grey) for all samples of this study. It is basically constant for all alignments and can serve as internal intensity reference allowing quantitative measurements independent of laser power.

Nevertheless, there are variations both in the extracted PDMS offset and the non-offset intensity as depicted in Fig. 4(b). This can have different reasons: laser power fluctuactions, analyte absorption and alignment uncertainties. In order to overcome all three obstacles, we propose to use the ratio P in Eq. (1), which compares non-offset to offset PDMS Raman intensity.

$$P = \frac{I_{\text{non-offset}}}{I_{\text{offset}}}\,. \tag{1}$$

Due to the simultaneous measurement of both intensities, the ratio P is independent of laser power fluctuactions. Furthermore, it is independent of analyte absorption as both intensities propagate through the channel and are consequently multiplied by the same absorption factor.

Optics EXPRESS

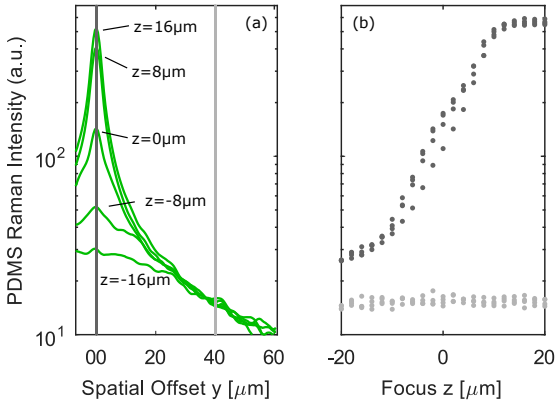

Fig. 4. (a) Comparison of PDMS Raman profiles (2920 cm^{-1}) at different focus positions z. (b) Z-scans of the $y = 40\,\mu$m spatially offset PDMS Raman intensity (light grey) as well as the PDMS Raman intensity at zero spatial offset (dark grey).

Last but not least, we claim that the ratio P is a good calibration measure for the optical alignment of the focus position z in the microfluidic channel. An alignment in this manner is advantageous compared to maximising the analyte Raman response.

Figure 5(a) plots the peak Raman intensity at 1375 cm^{-1} from an aqueous 1 g/l hemoglobin solution as a function of the focus position z which is moved across the microfluidic channel. One can clearly observe the alignment uncertainty in terms of z. In this protocol, we maximize the Raman peak intensity of hemoglobin, followed by a scan of z positions. The limited reproducibility of this optimization protocol can be explained by the flatness of the function for optimization, shown in Fig. 5(a). Furthermore, laser power and detected Raman peak count fluctuations make it difficult to find the precise maximum. Minor alignment drift of the flexible microfluidic chip with respect to the microscope objective during each z-scan leads to Raman peak intensity profiles of slightly varying shape.

In order to perform reproducible concentration measurements of the analyte in the microfluidic channel, it is essential always to align the optical system to the same z position. The highest sensitivity and the smallest errorbars can be achieved by a reproducible alignment in the middle of the channel. While the hemoglobin Raman peak intensity is flat in the vicinity of the maximum in the middle of the channel, the ratio P - as shown in Fig. 5(b) - is monotonically increasing as z is moved across the channel. Thus, a specific ratio P is unique for a specific z position, irrespective of analyte concentration. Therefore, P is a sensitive internal Raman measure which can be used for reproducible and precise optical alignment.

The PDMS Raman ratio P reports the alignment of the microfluidic chip with respect to the microscope. In Figs. 5(c-d) we demonstrate that the adjustment to a specific PDMS Raman ratio P is very reproducible in quantitative Raman experiments: For each of five different hemoglobin concentrations in the microfluidic channel, we move z to achieve a specific value of P. We then extract the respective Raman peak intensity at 1375 cm^{-1} and plot it as a function of hemoglobin concentration. The performed fit to a linear model is illustrated in Fig. 5(c) for $P = 5$. We use the *Matlab* routine *fitlm* [20] which outputs the fitted slope and its standard error. At various discrete values of P we perform sets of five concentration measurements, respectively. The sensitivity (slope) is the highest in the middle of the channel. The uncertainty (standard error) is the smallest where $P(z)$ has the greatest steepness.

Optics EXPRESS

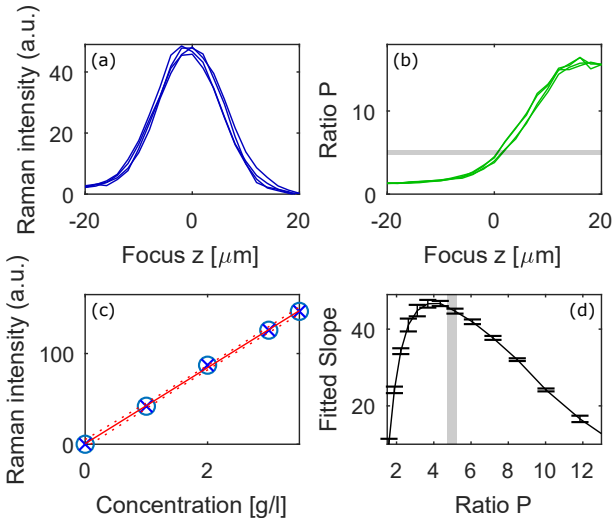

Fig. 5. (a) The amplitude of the hemoglobin Raman peak at 1375 cm^{-1} with 1 g/l in four repetitions. The focus position $z = 0\mu$ m is determined by maximizing the detected Raman amplitude, then a z-scan is performed. (b) The corresponding PDMS Raman ratio P of the same four repititions. (c) Five concentrations, with the optical system adjusted such that $P = 5$. (d) The derived slopes of the regression at various P values.

Beyond very good linearity and reproducibility, this alignment protocol has several strong points compared to an alignment protocol where the Raman peak intensity of hemoglobin would be maximized for each sample to reproduce a position z. As already mentioned, P is power independent as well as absorption independent and an internal measure for a specific objective-to-chip alignment. As P is measured simultaneously in the multispectral acquisition, there is potential for drift compensation, for example in a fixed Raman system or a Raman system without translation stage. The analyte intensity change due to drift can be corrected for by means of a calibrated model after data acquisition. As another advantage, the alignment can be done before the analyte arrives in the channel. Thus, there is no need for a long optimization on a sensitive analyte which could cause quenched Raman emission or could damage the analyte in other ways. With the proposed protocol, it is also possible to adjust to other z positions than the one where analyte Raman collection is maximized. This can be beneficial for example in the case of absorbing liquids or deep channels where alignment to the channel bottom is eventually of advantage.

4. Conclusion

In this study we combine SORS with microfluidics. We probe a two-layer system consisting of a 16 μm high microfluidic channel and extended PDMS chip material. The imaging spectrograph in connection with the optical microscope allows hyperspectral Raman acquisitions where Raman spectra are taken simultaneously along a continuum of spatial offsets with respect to the position of laser excitation. The Raman signatures of the two layers are easily distinguished as they are sufficiently separated in terms of their wavenumber. We investigate the different Raman contributions both spatially and spectrally for various positions z, the focus of the objective.

By extracting information from the spatially offset profile of the most dominant Raman line of PDMS in a z-scan, we find that the out-of-focus scattering results in a z-independent spatially

Optics EXPRESS

offset PDMS intensity. This is an absolute reference for Raman intensity and thus very valuable in quantitative Raman experiments. Furthermore, we find an internal reference measure for reproducible z alignment - the PDMS Raman ratio $P(z)$ - which is independent of laser power and analyte absorption. In general, $P(z)$ is not universal because it depends on channel depth, the depth of field of the microscope objective and the Raman microscope. However, this allows to adjust the characteristics of $P(z)$ for a specific need. In particular, one can establish a specific steepness of the PDMS Raman ratio $P(z)$ by modifying the channel depth and the depth of field of the microscope objective.

Through alignment to a specific $P(z)$, we demonstrate very consistent results for Raman concentration measurements of hemoglobin in aqueous solution. As the collected Raman intensity from the analyte in the channel strongly depends on the z position, it is important to reproduce the same z in a set of quantitative measurements. Alignment drift - in particular when liquid sample is exchanged - requires constant monitoring and control of the chip-to-objective distance. We argue that it is favorable to align to a specific value $P(z)$, rather than to optimize the analyte Raman collection. In contrast to the optimization protocol, our protocol allows the reproducible alignment to any focus position z which can be chosen such that it is most appropriate for the specific type of microfluidic Raman experiment.

Funding

Innovation Fund Denmark (5106-00015B).

Disclosures

The authors declare that there are no conflicts of interest related to this article.

References

1. N. Everall, T. Hahn, P. Matousek, A. W. Parker, and M. Towrie, "Photon Migration in Raman Spectroscopy," Appl. Spectrosc. **58**, 591–597 (2004).
2. P. Matousek, M. D. Morris, N. Everall, I. P. Clark, M. Towrie, E. Draper, A. Goodship, and A. W. Parker, "Numerical simulations of subsurface probing in diffusely scattering media using spatially offset Raman spectroscopy," Appl. Spectrosc **59**, 1485–1492 (2005).
3. P. Matousek, I. P. Clark, E. Draper, M. D. Morris, A. Goodship, N. Everall, M. Towrie, and A. W. Parker, "Subsurface probing in diffusely scattering media using spatially offset Raman spectroscopy," Appl. Spectrosc **59**, 393–400 (2005).
4. W. J. Olds, E. Jaatinen, P. Fredericks, B. Cletus, H. Panayiotou, and E. L. Izake, "Spatially offset Raman spectroscopy (SORS) for the analysis and detection of packaged pharmaceuticals and concealed drugs," Forensic Sci. Int. **212**, 69–77 (2011).
5. P. Matousek, C. Conti, M. Realini, and C. Colombo, "Micro-scale spatially offset Raman spectroscopy for non-invasive subsurface analysis of turbid materials," The Analyst **141**, 731–739 (2016).
6. C. Conti, C. Colombo, M. Realini, and P. Matousek, "Subsurface analysis of painted sculptures and plasters using micrometre-scale spatially offset raman spectroscopy (micro-sors)," J. Raman Spectrosc. **46**, 476–482 (2015).
7. C. Conti, M. Realini, C. Colombo, K. Sowoidnich, N. K. Afseth, M. Bertasa, A. Botteon, and P. Matousek, "Noninvasive analysis of thin turbid layers using microscale spatially offset Raman spectroscopy," Anal. Chem. **87**, 5810–5815 (2015).
8. Z. Di, B. H. Hokr, H. Cai, K. Wang, V. V. Yakovlev, A. V. Sokolov, and M. O. Scully, "Spatially offset Raman microspectroscopy of highly scattering tissue: Theory and experiment," J. Mod. Opt. **62**, 97–101 (2015).
9. M. D. Keller, R. H. Wilson, M. A. Mycek, and A. Mahadevan-Jansen, "Monte carlo model of spatially offset raman spectroscopy for breast tumor margin analysis," Appl. Spectrosc. **64**, 607–614 (2010).
10. Y. Cho, S. W. Song, J. Sung, Y.-S. Jeong, C. R. Park, and H. M. Kim, "Hyperspectral depth-profiling with deep Raman spectroscopy for detecting chemicals in building materials," The Analyst **142**, 3613–3619 (2017).
11. C. Conti, M. Realini, C. Colombo, and P. Matousek, "Comparison of key modalities of micro-scale spatially offset Raman spectroscopy," The Analyst **140**, 8127–8133 (2015).
12. J. Qin, M. S. Kim, W. F. Schmidt, B. K. Cho, Y. Peng, and K. Chao, "A line-scan hyperspectral Raman system for spatially offset Raman spectroscopy," J. Raman Spectrosc. **47**, 437–443 (2016).
13. A. F. Chrimes, K. Khoshmanesh, P. R. Stoddart, A. Mitchell, and K. Kalantar-zadeh, "Microfluidics and raman microscopy: current applications and future challenges," Chem. Soc. Rev. **42**, 5880–5906 (2013).

Optics EXPRESS

14. I. J. Jahn, O. Zukovskaja, X.-S. Zheng, K. Weber, T. W. Bocklitz, D. Cialla-May, and J. Popp, "Surface-enhanced raman spectroscopy and microfluidic platforms: challenges, solutions and potential applications," Analyst **142**, 1022–1047 (2017).
15. M. Matthiae, X. Zhu, R. Marie, and A. Kristensen, "In-line whole blood fractionation for Raman analysis of blood plasma," Analyst **144**, 602–610 (2019).
16. F. Adar, "Resonance Enhancement of Raman Spectroscopy: Friend or Foe?" Spectroscopy **28** (2013).
17. J. Qin, MS Kim, W. F. Schmidt, B-K. Cho, Y. Peng, and K Chao, "A line-scan hyperspectral raman system for spatially offset raman spectroscopy," J. Raman Spectrosc. **47**, 437–443 (2015).
18. T. G. Spiro, T.C. Streakas, "Hemoglobin: Resonance Raman spectra," Biochim. Biophys. Acta **263**, 830–833 (1972).
19. D. Cai, A. Neyer, R. Kuckuk, and H. M. Heise, "Raman, mid-infrared, near-infrared and ultraviolet visible spectroscopy of pdms silicone rubber for characterization of polymer optical waveguide materials," J. Mol. Struct. **976**, 274–281 (2010).
20. Matlab, *Version R2018a*, The MathWorks Inc. (2018).